THE JOURNAL OF PHYSICAL CHEMISTRY C
A JOURNAL OF THE AMERICAN CHEMICAL SOCIETY

pubs.acs.org/JPCC

Article

Tuning the Three-Phase Microenvironment Geometry Promotes Phase Formation

Guillermo S. Colón-Quintana, Kathryn J. Vannoy, Christophe Renault, Silvia Voci, and Jeffrey E. Dick*

Cite This: J. Phys. Chem. C 2022, 126, 20004−20010

Read Online

ACCESS | Metrics & More | Article Recommendations | Supporting Information

ABSTRACT: Nature builds multiphase environments to drive specific reactivity across boundaries. Multiphase systems present an opportunity to drive reactions that would otherwise not occur in bulk, continuous phases. Here, we demonstrate preferential nucleation near the three-phase boundary as a function of its geometry. A submicroliter water droplet deposited on an electrode immersed in a continuous 1,2-dichloroethane (DCE) phase is used to fabricate a three-phase junction (water|DCE|electrode). Adjusting the angle of the three-phase junction by changing the hydrophilicity of the electrode can lead to precipitation of ferrocenemethanol (FcMeOH) at the three-phase boundary only. Analysis by cyclic voltammetry coupled to numerical simulations provides insight into the physicochemical origin of the precipitation depending on the three-phase boundary angle. This finding offers a convenient means to control the local reactivity at three-phase boundaries.

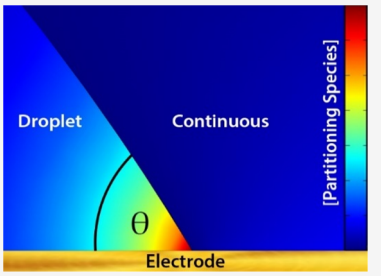

INTRODUCTION

Within the past decade, several groups have reported on unusual chemical reactivity in microenvironments by studying submicroliter volumes with various analytical techniques. Marken and co-workers have taken advantage of this unusual reactivity to promote useful electro-organic multiphase reactions.[1] Cooks and co-workers have studied a variety of organic reactions in electrospray droplets and discovered that reaction rates are accelerated[2−9] and demonstrated the importance of analyte solvation at the air|water interface.[10] Zare and co-workers have shown spontaneous reduction occurs at the boundary of water microdroplets surrounded by air.[12,13] Pielak and co-workers have demonstrated protein stability is decreased in inverse micelles compared to studies in a bulk buffer.[11]

In the experiments described above, one cannot rule out the role adsorption plays in small volumes. The smaller the droplet, the more the analyte has access to the surface. Griffiths and Wilson have independently demonstrated that chemical reactions can accelerate in micron-sized compartments due to interfacial adsorption.[14,15] A necessary complication in electrochemical measurements of reactions in small volumes is that electrochemistry requires electrodes (solid|liquid interfaces). Thus, a three-phase boundary comprised of the electrode, droplet, and continuous phase is formed. Using voltammetry, one can probe physicochemical properties and processes occurring at the three-phase boundary of single microliter droplets and arrays of microdroplets.[16−19] Scholz and co-workers have explored heterogeneous chemistry in immobilized droplets and derived robust thermodynamic and kinetic values.[20−22] Compton and coauthors have also thoroughly investigated such systems[18,23−25] and used numerical simulations to interpret their observations.[26] In recent years, our group has observed chemistry that is localized to the three-phase boundary of femtoliter-microliter droplets and shown the preferential electroreduction at the oil|water|conductor (three-phase) interface.[27−30] White and co-workers studied the transfer of ferrocene from a 1,2-dichloroethane (DCE) oil phase to an aqueous phase along an electrode traversing both phases.[31] They evidenced that ferrocenium electrogenerated at the DCE|electrode boundary near the three-phase boundary is able to cross the water|DCE boundary and be reduced back to ferrocene at the water|electrode interface. Based on numerical simulation, the authors demonstrate that diffusion of the species is rate determining compared to oxidation, reduction, and phase transfer kinetics. Interestingly, simulations reveal that the diffusion layers of the electrogenerated species directly in the vicinity of the three-phase boundary are drastically affected by the adjacent phase transfer. The authors performed simulations for different geometries and evidence that the curvature of the three-phase boundary should influence the magnitude of the peak current associated with the voltammetry of ferrocene in the water phase. Nonetheless, no physical insight is drawn from the simulations. A similar study by Scholz and co-workers uses a wire electrode spanning through a nitrobenzene droplet immersed in an aqueous solution, and reveals that precipitation of decamethylferrocenium nitrate salt can occur at the three-phase boundary.[32] The authors explore

Received: June 8, 2022
Revised: August 22, 2022
Published: November 18, 2022

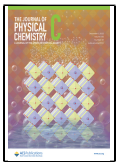

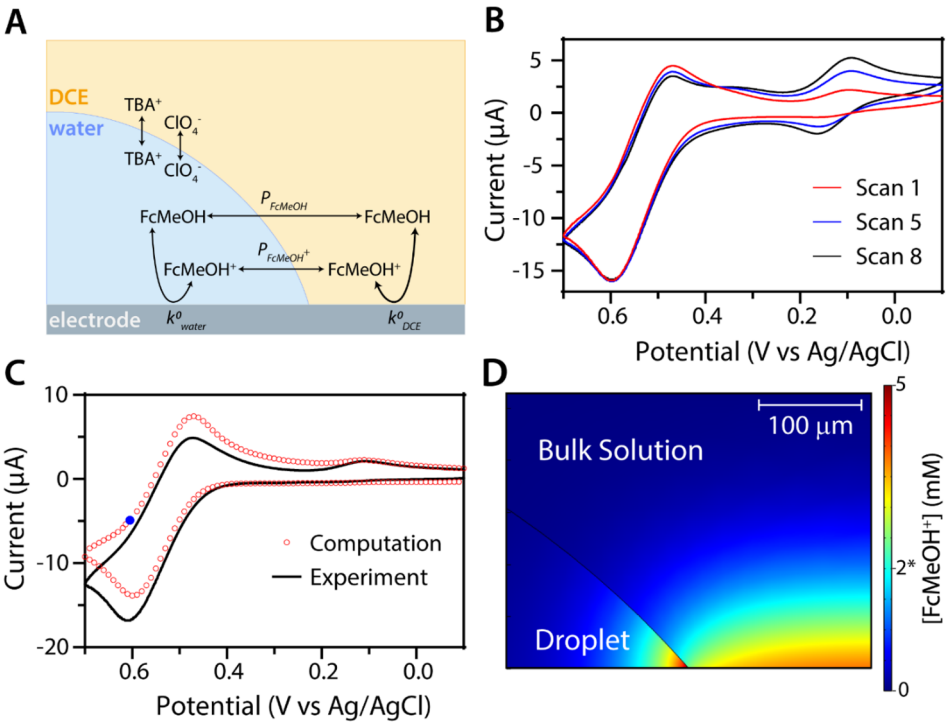

Figure 1. (A) Scheme of the electrochemical system representing a water droplet (blue color) sitting on top of a macroelectrode and immersed in DCE (yellow color). The redox reactions and phase transfer reactions are indicated with double sided arrows denoting reversible processes. All species are freely diffusing in both phases. (B) CVs recorded with a 500 nL 0.1 M TBACl droplet pipetted onto a 1 mm radius gold electrode and immersed in continuous DCE phase containing 0.1 M $TBAClO_4$ and 4 mM FcMeOH. The red, blue, and black traces correspond to the first, fifth, and eighth consecutive scans, respectively. Scan rate is 50 mV/s. (C) Experimental (black trace) and simulated (red circles) CVs. The black trace is the same as the red one shown in Figure 1B. The simulated CV is obtained by solving numerically the diffusion of FcMeOH and $FcMeOH^+$ species, while the latter is being produced/consumed at the electrode surface. Phase transfer of the species between DCE and water is considered to be at equilibrium. See main text and Supporting Information for further details about the simulation. (D) Concentration profile of $FcMeOH^+$ simulated at 18 s (0.6 V on the backward scan) of the CV shown in Figure 1C (indicated by the blue dot). The solubility of FcMeOH (the neutral counterpart) is given on the scale bar with an asterisk.

how the concentration and solubility of the counterion (ClO_4^-, NO_3^-, Cl^-) in both phases affect the extent of the precipitation. The geometry of the interface is not considered in their work.

In our work, we use electrochemical reactions to both trigger large concentration gradients of species in one phase and detect the transfer of these species in the other phase. Cyclic voltammetry in conjunction with optical observation of the three-phase boundary is used to track the formation of a new phase at the three-phase boundary. In this manuscript, we show and explain based on numerical simulations how precipitation can be promoted simply by changing the microenvironment geometry at the three-phase boundary.

RESULTS AND DISCUSSION

Figure 1A shows a scheme of the electrochemical system under investigation. A 500 nL water droplet containing 0.1 M of tetrabutylammonium (TBA^+) chloride is sitting on a 1 mm radius gold (Au) electrode. The electrode and the water droplet are immersed in DCE containing 4 mM of FcMeOH and 0.1 M of tetrabutylammonium perchlorate ($TBAClO_4$). A Ag/AgCl 1 M KCl reference electrode is connected to the cell through a salt bridge. A 0.5 mm radius glassy carbon rod is used a counter electrode. The potential of the working electrode can be adjusted to drive the one-electron oxidation/reduction of the FcMeOH and $FcMeOH^+$, respectively. This redox process is indicated by the curved arrows in Figure 1A. The geometry of the droplet depends on the hydrophilicity of the electrode surface and how gently the droplet is pipetted onto the surface. The contact angle at the three-phase boundary is thus systematically measured by taking optical micrographs (cf. Figure S1 in Supporting Information) of the 500 nL droplet after immersed in the DCE phase. For a Au surface, the contact angle is about 57° leading to the droplet|electrode interface having a radius of 678 μm and a droplet height of 307 μm. The first and eighth consecutive cyclic voltammograms (CVs) recorded with this system are shown in Figure 1B in red and black colors, respectively. On the red trace, only one pair of an anodic and cathodic peak centered at $E_{1/2}^{DCE}$ = 0.53 V *vs* Ag/AgCl is observed. The black trace shows not only the first pair of peaks but also a second pair of anodic and cathodic peaks centered at $E_{1/2}^{water}$ = 0.13 V *vs* Ag/AgCl. This second pair of peaks grows in intensity as the number of scans increases, while the intensity of the peaks for the first pair stays relatively constant. The peak splitting for the first and second pairs of peaks are 140 and 60 mV, respectively. CVs recorded in the water or DCE phases containing FcMeOH (see Figure S2 in Supporting Information) show only one pair of reversible peaks. The oxidation/reduction of FcMeOH/$FcMeOH^+$ in DCE and water are centered at 0.60 V *vs* Ag/AgCl and 0.22 V *vs* Ag/AgCl, respectively. Thus, we attribute the two pairs of peaks to the reversible oxidation/reduction of FcMeOH/$FcMeOH^+$ at the DCE|electrode and water|electrode interfaces. Oxidation of FcMeOH in the water

https://doi.org/10.1021/acs.jpcc.2c03973
J. Phys. Chem. C 2022, 126, 20004−20010

phase occurs about 380 mV earlier than in the DCE phase. The shift comes from both the difference in formal potentials in the water and DCE phases as well as an eventual liquid|liquid junction potential.[33] Our observation is in agreement with the results of White and co-workers who also observed two pairs of peaks when using a wire electrode crossing a water phase and a DCE phase containing ferrocene.[31] We observe the appearance of the second pair of peak only after the first scan, as they do.

The shape of the CVs can be explained as follows. During the initial sweep, the concentration of FcMeOH in the water droplet is too low to produce a visible faradaic peak in the CV. However, the oxidation of the 4 mM of FcMeOH contained in the DCE continuous phase leads to a large anodic peak (centered at 0.6 V *vs* Ag/AgCl in Figure 1B) followed by a cathodic peak (centered at 0.47 V *vs* Ag/AgCl in Figure 1B). At about 0.1 V *vs* Ag/AgCl, a cathodic peak corresponding to the reduction of $FcMeOH^+$ in the water phase is observed. Only on the subsequent scans is an anodic peak is observed in water. We conclude that a measurable amount of $FcMeOH^+$ is transferred from the DCE to the water phase during the course of the voltammetric experiment. The transfer of the various freely diffusing species across the DCE|water interface is represented by the straight arrows in Figure 1A. The charge balance must be enforced by either the transfer of TBA^+ from water to DCE or ClO_4^- from DCE to water. The TBA^+ and ClO_4^- ions have similar standard Gibbs free energies of ion transfer (−226 and −178 mV, respectively), and both are expected to cross the interface.[33] The transfer of the counter charges is represented in Figure 1A with vertical arrows.

This mechanism was tested quantitatively by simulating the CVs. The kinetics of oxidation/reduction of FcMeOH/$FcMeOH^+$ at the DCE|electrode and water|electrode interfaces, their diffusion in both phases, as well as their partitioning at the DCE|water interface were simulated by a finite element method. Kinetics of electron transfer are represented with a Butler−Volmer law, while diffusion obeys Fick's second law. The partitioning at the DCE|water interface is implemented with two first-order kinetics for each species. The first and second kinetics represent the transfer from water to DCE and DCE to water, respectively. The ratio of the two kinetic parameters is equal to the partition constant. For the sake of simplicity, the polarization of the liquid|liquid interface is not simulated, and electroneutrality is assumed at all times. Despite these assumptions, a large number of parameters are present in the simulation. We tried to fix as many parameters as possible. The initial concentrations of species in both phases ($[FcMeOH^+]_{DCE}$ = 0 mM, $[FcMeOH^+]_{water}$ = 0 mM, $[FcMeOH]_{DCE}$ = 4 mM, $[FcMeOH^+]_{water}$ = 0 mM) are set by the amount of species initially added in solution. Their diffusion coefficients ($D^{DCE}_{FcMeOH} = D^{water}_{FcMeOH} = 7.00 \times 10^{-6}$ cm^2·s^{-1} and $D^{DCE}_{FcMeOH^+} = D^{water}_{FcMeOH^+} = 8.89 \times 10^{-6}$ cm^2·s^{-1}) were experimentally measured for water and DCE. Their partition coefficients (P_{FcMeOH} = 71 and P_{FcMeOH^+} = 0.5) were measured independently (see Figure S3 in Supporting Information) and thus are fixed parameters of the simulation. The standard rate constant for electron transfer at the water|electrode interface and symmetry coefficients are also fixed (k°_{water} = 10 cm·s^{-1} and α = 0.5) based on literature values.[34] Measurements of CVs in DCE (see CV in Figure S4) with 1 mM FcMeOH and 0.1 M $TBAClO_4$ show a Nernstian behavior at 0.05 V/s with D_{FcMeOH} = 8.89 × 10^{-6} cm^2·s^{-1}. Thus, k°_{DCE} must be larger than $\sim 10 \times \sqrt{FDv/RT}$, which is about 0.0004 cm/s.[35] We use k°_{DCE} = 10 cm·s^{-1}. Since the kinetics of electron transfer at the DCE|electrode interface is not rate determining in our experiment, we simply assumed α = 0.5. The only free parameters are the kinetics of FcMeOH/$FcMeOH^+$ crossing the water|DCE interfaces. Note that the ratio of these two kinetic parameters is the partition coefficient, a fixed parameter. We also note that the large peak splitting of the pair of peaks centered at 0.53 V *vs* Ag/AgCl observed in Figure 1B,C (black traces) is attributed to ohmic drop. Serial resistance is commonly encountered in low dielectric solvents like DCE. A 2 kΩ serial resistance was introduced in the numerical simulation to account for the peak splitting. More details about the simulation are provided in Supporting Information.

Figure 1C shows the experimental (black trace) and simulated (red circles) CVs (first scans). The experimental CV is subtracted from a blank measured in absence of FcMeOH (Figure S5 in Supporting Information). The oxidation/reduction of FcMeOH/$FcMeOH^+$ in DCE is well reproduced by the simulation. The simulation also correctly predicts the appearance of a second cathodic peak on the reverse scan (at 0.10 V *vs* Ag/AgCl). We observed that experimental CVs are well reproduced only when diffusion is the limiting step (with respect to electron transfer and partitioning). This observation is in agreement with results obtained by White and co-workers using ferrocene.[31] The concentration profile of $FcMeOH^+$ at 0.6 V *vs* Ag/AgCl on the reverse scan (indicated by the blue dot in Figure 1C) is shown in Figure 1D. At this potential, FcMeOH is oxidized at the DCE|electrode interface as indicated by the concentration gradient developing along this interface (orange to blue color gradient normal to the interface). The dark blue color near the center of the droplet indicates that $FcMeOH^+$ is not produced at the water|electrode interface.

However, at the three-phase boundary, a large concentration of $FcMeOH^+$ is observed in the water phase (red−orange colors), while the concentration in the DCE phase drops (green color). This indicates that $FcMeOH^+$ produced in the DCE phase transfers to the water phase. The transferred $FcMeOH^+$ can then be reduced at the water|electrode interface near the three-phase boundary giving rise to the second cathodic peak at 0.10 V *vs* Ag/AgCl on the CVs.

Scholz and co-workers showed that the transfer of species from one phase to another may be accompanied by side reactions like precipitation.[32] We investigated that possibility by performing chronoamperometric experiments coupled with optical observations of the three-phase boundary. Figure 2A,B shows the sequence of potential, and the resulting current flowing through a platinum (Pt) electrode with a 500 nL water droplet containing 0.1 M of TBACl immersed in a continuous DCE phase containing 40 mM of FcMeOH and 1 M of $TBAClO_4$. These high concentrations of species are used to ease the visualization of the precipitate. First, the electrode is held 3.5 s at 0.7 V *vs* Ag/AgCl ($>E^{water}_{1/2}$ and $>E^{DCE}_{1/2}$) to drive the oxidation of FcMeOH in the DCE phase and transfer of $FcMeOH^+$ toward the water droplet. Then, a potential of -0.1 V *vs* Ag/AgCl ($<E^{water}_{1/2}$ and $E^{DCE}_{1/2}$) is held to drive the reduction of $FcMeOH^+$ in both the DCE and water phases. Top view optical micrographs centered on the three-phase boundary and recorded at the end of the anodic (Figure 2A) and cathodic (Figure 2B) pulses are shown in Figure 2C,D, respectively. The left side light gray of the micrographs corresponds to the area above the water droplet, while the darker gray area on the right of the micrographs corresponds to the DCE phase. The long

https://doi.org/10.1021/acs.jpcc.2c03973
J. Phys. Chem. C 2022, 126, 20004−20010

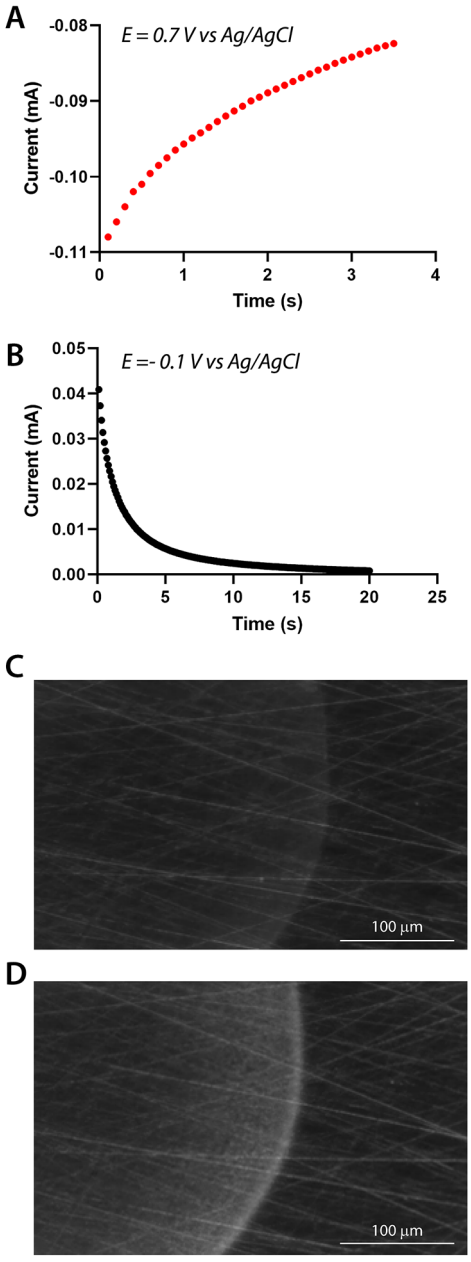

Figure 2. Chronoamperometric experiment performed for the oxidation of FcMeOH (A) and reduction (B) of $FcMeOH^+$ in both phases. A 500 nL aqueous droplet containing 0.1 M TBACl was deposited onto a 1 mm radius Pt electrode and immersed in a DCE continuous phase containing 40 mM FcMeOH and 1 M $TBAClO_4$. Optical micrographs of the droplet in (C) and (D) are taken after 3.5 s at 0.7 V *vs* Ag/AgCl shown in (A) and 20 s at -0.1 V *vs* Ag/AgCl shown in (B), respectively. The scale bars represent 100 μm. On the micrograph (D), a white ring appears at the three-phase boundary. This ring is attributed to the formation of FcMeOH crystals.

oblique lines are scratches on the metal surface caused during polishing. Both the water and DCE phases are transparent during the anodic pulse. However, the water phase near the three-phase boundary becomes cloudy as the reduction of $FcMeOH^+$ proceeds. We attribute this cloudiness to the scattering of light by large particles of solid formed near the interface. When we apply an intermediate potential of 0.4 V *vs* Ag/AgCl, which is sufficient to reduce $FcMeOH^+$ in the DCE phase (>0.53 V *vs* Ag/AgCl) but not in the water phase (>0.13 V *vs* Ag/AgCl), we do not observe formation of a precipitate (Figure S6 in Supporting Information). The formation of a precipitate is observed only during the reduction of $FcMeOH^+$ in water. We conclude that FcMeOH precipitates in the water phase.

The precipitation of FcMeOH near the three-phase boundary is explained as follows. We showed in Figure 1D that a large concentration of $FcMeOH^+$ can build up in the water phase near the three-phase boundary. When this large concentration of $FcMeOH^+$ is suddenly reduced back to the much less soluble FcMeOH species, the latter precipitates.

Precipitation of the reduced form of the redox couple is in contrast with the observation of Scholz and co-workers where electrogenerated decamethylferrocenium forms an insoluble salt with an anion present in either the water or organic phase.[32] We verified that such a reaction can also occur in our system by adding phosphate in the water phase and observing the precipitation of $FcMeOH^+H_2PO_4^-$ near the three-phase boundary (see Figure S7 in Supporting Information). Interestingly, our experiments with only $TBAClO_4$ (in DCE) and TBACl (in water) show that these salts do not participate in the formation of a new phase. Even though TBA^+ cation is known to act as a phase transfer catalyst by forming a complex with some anions, we do not expect positively charged TBA^+ to aid the phase transfer of positively charged $FcMeOH^+$.[36]

The formation of a solid phase of FcMeOH requires some specific conditions. Nucleation takes a certain amount of time and depends on the competition between the birth rate and death rate of the first nucleus.[37] This time is called the induction time. In our experiments, the voltammetric sweep rate must be slower than the induction time but faster than diffusion, to promote the nucleation of a new phase. While precipitation of FcMeOH is a special case, one must consider the nucleation induction period when translating the current work to other systems. However, using this model, one can adjust experimental parameters in this system to predict concentrations that would lead to the precipitation of FcMeOH. Observation of precipitation requires maintaining a concentration of FcMeOH larger than the solubility limit for a time longer than the induction time. These conditions can be achieved by adjusting the initial concentration of FcMeOH and the duration of the electrogeneration of $FcMeOH^+$. Besides these two obvious parameters, we should also consider another parameter, the geometry of the three-phase boundary. Indeed, building up a large concentration of $FcMeOH^+$ in the water phase is intimately related to the diffusion profiles of the species near the three-phase boundary. The geometry of this interface can favor or disfavor accumulation of species. In our experiments, the wetting of the droplet can drastically affect the geometry near the three-phase boundary. Figure 3A,B shows side view optical micrographs of water droplets deposited onto a 1 mm radius Pt electrode and a 1.5 mm radius glassy carbon electrode, respectively. The contact angles on the Pt and glassy carbon are 58 and 121°, respectively. The 500 nL water droplets contained 0.1 M TBACl, while the DCE continuous phase contained 40 mM FcMeOH and 1 M $TBAClO_4$. The potential was swept at 50 mV/s from −0.1 to 0.7 V *vs* Ag/AgCl and back to −0.1 V *vs* Ag/AgCl. We observe no precipitate rings on glassy carbon by optical inspection of the surface during the course of the voltammetry. On the other hand, we do observe precipitation on the Pt surface (as it was observed in Figure 2 by chronoamperometry). To provide physical insight, we performed numerical simulations of CVs in

https://doi.org/10.1021/acs.jpcc.2c03973
J. Phys. Chem. C 2022, 126, 20004−20010

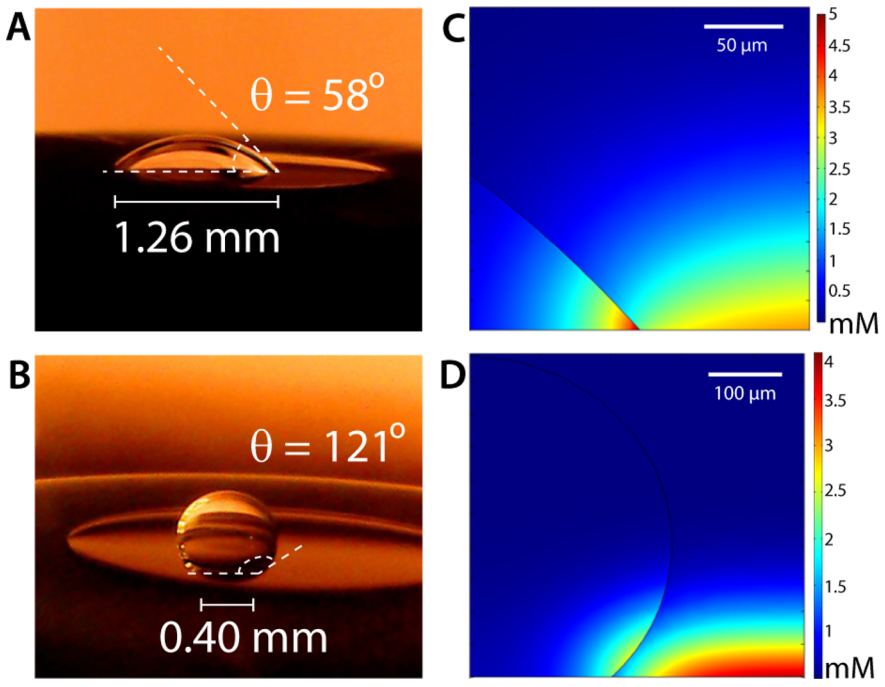

Figure 3. (A,B) Side view optical micrographs of a water droplet pipetted onto a Pt and glassy carbon electrode, respectively. Due to the difference in wettability of these two surfaces, the contact angle varies from 58 to 121°. (C,D) Concentration profiles of $FcMeOH^+$ simulated for CVs in the same conditions as in Figure 1D but using a droplet geometry corresponding to (A) and (B), respectively. The difference in contact angle drastically affects the concentration profile near the three-phase boundary.

these two different geometries. All the parameters of the simulation are identical to the ones used in Figure 1B, except the initial concentration of FcMeOH in the DCE phase and the geometry of the droplet.

Concentration profiles of $FcMeOH^+$ for the 58 and 121° angles are shown in Figure 3C and D, respectively. A striking difference in the maximum concentration of $FcMeOH^+$ near the three-phase boundary is observed. The concentration of FcMeOH at the three-phase boundary (in the water phase) is about 2.5 times larger for an angle of 58° than for an angle of 121°. This difference can be understood as follows. A low angle produces a geometry that resembles a channel in the water phase. A narrow shape favors the intake of $FcMeOH^+$ from the DCE to the water phase while hindering the diffusion of the $FcMeOH^+$ from the three-phase boundary toward the center of the droplet.

The concentration of $FcMeOH^+$ accumulated at the three-phase boundary as a function of the angle of the three-phase boundary is shown in Figure 4. Here, the simulated concentration in the water phase was taken 10 nm from the three-phase contact and is used to represent a trends 2D plot. The concentration of $FcMeOH^+$ accumulated in the water phase near the three-phase boundary increases dramatically from 2 mM at 131° to 8 mM at 2.5°. Figure 4 also shows that about 80% of the variation of concentration occurs when the angles vary from 10 to 100°. Besides these values, the concentration does not vary significantly. In a nutshell, when the contact angle decreases, the local concentration of transferred species increases at the three-phase microenvironment. This observation can shed light on previous work in the literature. White and co-workers performed numerical simulations of CVs at three different DCE|water|electrode contact angles and predicted a variation of the peak current for the oxidation of the species accumulated in the water phase

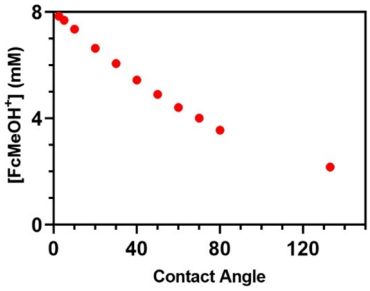

Figure 4. Concentration of $FcMeOH^+$ in the water phase simulated at 10 nm from the three-phase boundary during the course of a CV as described in Figure 1B. Several simulations are performed for different contact angles representing a wetting (<90°) and nonwetting (>90°) droplet. [$FcMeOH^+$] is simulated at 0.6 V *vs* Ag/AgCl, 18 s into a CV from 0.7 to -0.1 V *vs* Ag/AgCl.

(ferrocenium in their case). However, no physical insight was provided to account for this prediction. Based on our findings, we propose that the peak current will vary because the amount of species accumulated in the water phase depends on the geometry of the three-phase boundary.

In conclusion, we have demonstrated that phase nucleation can be favored in multiphase systems based on simple geometrical considerations. Based on numerical simulations of CVs, we clearly evidence that diffusion limited phase transfer is the cause of large concentration gradients near the three-phase boundary. Importantly, we evidence that low contact angles favor high concentrations of species in the droplet near the three-phase boundary. We prove that a careful design of the three-phase boundary geometry can be used to trigger local precipitation of FcMeOH. Our results are generalizable to a heterogeneous reaction that creates a product that may be more soluble in the droplet phase (for

https://doi.org/10.1021/acs.jpcc.2c03973
J. Phys. Chem. C 2022, 126, 20004−20010

instance, the heterogeneous reduction of CO_2 to formate, which is much more soluble in an aqueous droplet).[38] The reach of our finding is not limited to precipitation and can be extended to other reactions such as bimolecular chemical reactions, which should see their kinetics strongly affected by the local geometry.

■ ASSOCIATED CONTENT

Supporting Information

The Supporting Information is available free of charge at https://pubs.acs.org/doi/10.1021/acs.jpcc.2c03973.

Chemicals and methods, droplet size and contact and angle measurements, controls for the voltammetry of FcMeOH in bulk solutions, partition coefficient measurements, simulated and nonsimulated voltammetry, precipitation studies, and numerical simulations with simulation report (PDF)

■ AUTHOR INFORMATION

Corresponding Author

Jeffrey E. Dick − *Department of Chemistry and Lineberger Comprehensive Cancer Center, The University of North Carolina at Chapel Hill, Chapel Hill, North Carolina 27599, United States;* orcid.org/0000-0002-4538-9705; Email: jedick@email.unc.edu

Authors

Guillermo S. Colón-Quintana − *Department of Chemistry, The University of North Carolina at Chapel Hill, Chapel Hill, North Carolina 27599, United States*

Kathryn J. Vannoy − *Department of Chemistry, The University of North Carolina at Chapel Hill, Chapel Hill, North Carolina 27599, United States;* orcid.org/0000-0002-5723-9755

Christophe Renault − *Physique de la Matière Condensée, CNRS, Ecole Polytechnique, 91128 Palaiseau, France;* orcid.org/0000-0003-4525-8702

Silvia Voci − *Department of Chemistry, The University of North Carolina at Chapel Hill, Chapel Hill, North Carolina 27599, United States*

Complete contact information is available at: https://pubs.acs.org/10.1021/acs.jpcc.2c03973

Author Contributions

GSCQ and KJV contributed equally to this work.

Author Contributions

JED, KJV, and GSCQ conceived the work. JED, KJV, GSCQ, and CR participated in experimental design and data analysis/interpretation. GSCQ performed electrochemical experiments with input from KJV and JED. SV performed experiments on the inverted microscope. GSCQ, KJV, CR, and JED designed the finite element model. All authors participated in manuscript preparation. JED supervised all aspects of the research.

Notes

The authors declare no competing financial interest.

■ ACKNOWLEDGMENTS

This work was completed with financial support from the Chemical Measurement and Imaging Program in the National Science Foundation Division of Chemistry under Grant CHE-2003587.

■ REFERENCES

(1) Marken, F.; Wadhawan, J. D. Multiphase Methods in Organic Electrosynthesis. *Acc. Chem. Res.* **2019**, *52*, 3325−3338.

(2) Wei, Z.; Wleklinski, M.; Ferreira, C.; Cooks, R. G. Reaction Acceleration in Thin Films with Continuous Product Deposition for Organic Synthesis. *Angew. Chem., Int. Ed.* **2017**, *56*, 9386−9390.

(3) Müller, T.; Badu-Tawiah, A.; Cooks, R. G. Accelerated Carbon-Carbon Bond-Forming Reactions in Preparative Electrospray. *Angew. Chem., Int. Ed.* **2012**, *51*, 11832−11835.

(4) Badu-Tawiah, A. K.; Campbell, D. I.; Cooks, R. G. Accelerated C-N bond formation in dropcast thin films on ambient surfaces. *J. Am. Soc. Mass Spectrom.* **2012**, *23*, 1461−8.

(5) Yan, X.; Augusti, R.; Li, X.; Cooks, R. G. Chemical Reactivity Assessment Using Reactive Paper Spray Ionization Mass Spectrometry: The Katritzky Reaction. *ChemPlusChem.* **2013**, *78*, 1142−1148.

(6) Li, Y.; Yan, X.; Cooks, R. G. The Role of the Interface in Thin Film and Droplet Accelerated Reactions Studied by Competitive Substituent Effects. *Angew. Chem., Int. Ed. Engl.* **2016**, *55*, 3433−7.

(7) Girod, M.; Moyano, E.; Campbell, D. I.; Cooks, R. G. Accelerated bimolecular reactions in microdroplets studied by desorption electrospray ionization mass spectrometry. *Chemical Science* **2011**, *2*, 501−510.

(8) Bain, R. M.; Pulliam, C. J.; Raab, S. A.; Cooks, R. G. Chemical Synthesis Accelerated by Paper Spray: The Haloform Reaction. *J. Chem. Educ.* **2016**, *93*, 340−344.

(9) Bain, R. M.; Pulliam, C. J.; Cooks, R. G. Accelerated Hantzsch electrospray synthesis with temporal control of reaction intermediates. *Chemical Science* **2015**, *6*, 397−401.

(10) Qiu, L.; Wei, Z.; Nie, H.; Cooks, R. G. Reaction Acceleration Promoted by Partial Solvation at the Gas/Solution Interface. *ChemPlusChem.* **2021**, *86*, 1362−1365.

(11) Senske, M.; Smith, A. E.; Pielak, G. J. Protein Stability in Reverse Micelles. *Angew. Chem., Int. Ed. Engl.* **2016**, *55*, 3586−9.

(12) Lee, J. K.; Walker, K. L.; Han, H. S.; Kang, J.; Prinz, F. B.; Waymouth, R. M.; Nam, H. G.; Zare, R. N. Spontaneous generation of hydrogen peroxide from aqueous microdroplets. *Proc. Natl. Acad. Sci. U. S. A.* **2019**, *116*, 19294.

(13) Lee, J. K.; Samanta, D.; Nam, H. G.; Zare, R. N. Micrometer-Sized Water Droplets Induce Spontaneous Reduction. *J. Am. Chem. Soc.* **2019**, *141*, 10585−10589.

(14) Fallah-Araghi, A.; Meguellati, K.; Baret, J.-C.; Harrak, A. E.; Mangeat, T.; Karplus, M.; Ladame, S.; Marques, C. M.; Griffiths, A. D. Enhanced Chemical Synthesis at Soft Interfaces: A Universal Reaction-Adsorption Mechanism in Microcompartments. *Phys. Rev. Lett.* **2014**, *112*, No. 028301.

(15) Wilson, K. R.; Prophet, A. M.; Rovelli, G.; Willis, M. D.; Rapf, R. J.; Jacobs, M. I. A kinetic description of how interfaces accelerate reactions in micro-compartments. *Chemical Science* **2020**, *11*, 8533−8545.

(16) Tasakorn, P.; Chen, J.; Aoki, K. Voltammetry of a single oil droplet on a large electrode. *J. Electroanal. Chem.* **2002**, *533*, 119−126.

(17) Aoki, K.; Satoh, M.; Chen, J.; Nishiumi, T. Convection caused by three-phase boundary reactions. *Journal of Electroanalytical Chemistry - J. ELECTROANAL CHEM* **2006**, *595*, 103−108.

(18) Davies, T. J.; Wilkins, S. J.; Compton, R. G. The electrochemistry of redox systems within immobilised water droplets. *J. Electroanal. Chem.* **2006**, *586*, 260−275.

(19) Chen, J.; Ikeda, O.; Aoki, K. Electrode reaction of ferrocene in a nitrobenzene+water emulsion. *J. Electroanal. Chem.* **2001**, *496*, 88−94.

(20) Scholz, F.; Schröder, U.; Gulaboski, R.*Electrochemistry of Immobilized Particles and Droplets*, 1st ed.; Springer: Berlin, 2005.

(21) Scholz, F.; Komorsky-Lovrić, Š.; Lovrić, M. A new access to Gibbs energies of transfer of ions across liquidlliquid interfaces and a new method to study electrochemical processes at well-defined three-phase junctions. *Electrochem. Commun.* **2000**, *2*, 112−118.

(22) Hermes, M.; Scholz, F. The electrochemical oxidation of white phosphorus at a three-phase junction. *Electrochem. Commun.* **2000**, *2*, 845−850.

(23) Banks, C. E.; Davies, T. J.; Evans, R. G.; Hignett, G.; Wain, A. J.; Lawrence, N. S.; Wadhawan, J. D.; Marken, F.; Compton, R. G. Electrochemistry of immobilised redox droplets: Concepts and applications. *Phys. Chem. Chem. Phys.* **2003**, *5*, 4053−4069.
(24) Kätelhön, E.; Tanner, E. E. L.; Batchelor-McAuley, C.; Compton, R. G. Destructive nano-impacts: What information can be extracted from spike shapes? *Electrochim. Acta* **2016**, *199*, 297−304.
(25) Wadhawan, J. D.; Evans, R. G.; Banks, C. E.; Wilkins, S. J.; France, R. R.; Oldham, N. J.; Fairbanks, A. J.; Wood, B.; Walton, D. J.; Schröder, U.; Compton, R. G. Voltammetry of Electroactive Oil Droplets: Electrochemically-Induced Ion Insertion, Expulsion and Reaction Processes at Microdroplets of N,N,N‘,N‘-Tetraalkyl-para-phenylenediamines (TRPD, R = n-Butyl, n-Hexyl, n-Heptyl and n-Nonyl). *J. Phys. Chem. B* **2002**, *106*, 9619−9632.
(26) Ball, J. C.; Marken, F.; Fulian, Q.; Wadhawan, J. D.; Blythe, A. N.; Schröder, U.; Compton, R. G.; Bull, S. D.; Davies, S. G. Voltammetry of Electroactive Oil Droplets. Part II: Comparison of Experimental and Simulation Data for Coupled Ion and Electron Insertion Processes and Evidence for Microscale Convection. *Electroanalysis* **2000**, *12*, 1017−1025.
(27) Glasscott, M. W.; Voci, S.; Kauffmann, P. J.; Chapoval, A. I.; Dick, J. E. Mapping Solvent Entrapment in Multiphase Systems by Electrogenerated Chemiluminescence. *Langmuir* **2021**, *37*, 2907−2912.
(28) Reyes-Morales, J.; Glasscott, M. W.; Pendergast, A. D.; Goines, S.; Dick, J. E. The oxidation of ferrocene in sessile toluene macro- and microdroplets: An opto-electrochemical study. *J. Electroanal. Chem.* **2022**, *905*, 115922.
(29) Clarke, T. B.; Dick, J. E. Preferential Electroreduction at the Oil|Water|Conductor Interface. *J. Phys. Chem. Lett.* **2022**, *13*, 3338−3341.
(30) Terry Weatherly, C. K.; Glasscott, M. W.; Dick, J. E. Voltammetric Analysis of Redox Reactions and Ion Transfer in Water Microdroplets. *Langmuir* **2020**, *36*, 8231−8239.
(31) Terry Weatherly, C. K.; Ren, H.; Edwards, M. A.; Wang, L.; White, H. S. Coupled Electron- and Phase-Transfer Reactions at a Three-Phase Interface. *J. Am. Chem. Soc.* **2019**, *141*, 18091−18098.
(32) Donten, M.; Bak, E.; Gniadek, M.; Stojek, Z.; Scholz, F. Three-phase electrochemistry with a hanging drop of water-insoluble liquid: Precipitation of decamethylferrocenium species as a marker of ion transfer route. *Electrochim. Acta* **2008**, *53*, 5608−5614.
(33) Markin, V. S.; Volkov, A. G. The gibbs free energy of ion transfer between two immiscible liquids. *Electrochim. Acta* **1989**, *34*, 93−107.
(34) Sun, P.; Mirkin, M. V. Kinetics of Electron-Transfer Reactions at Nanoelectrodes. *Anal. Chem.* **2006**, *78*, 6526−6534.
(35) Bard, A. J.; Faulkner, L. R.*ELECTROCHEMICAL METHODS Fundamentals and Applications*, 2nd ed.; Wiley, 2000.
(36) Ohtani, N.; Ohta, T.; Hosoda, Y.; Yamashita, T. Phase Behavior and Phase-Transfer Catalysis of Tetrabutylammonium Salts. Interface-Mediated Catalysis. *Langmuir* **2004**, *20*, 409−415.
(37) Abyaneh, M. Y.; Fleischmann, M.; Del Giudice, E.; Vitiello, G. The investigation of nucleation using microelectrodes: I. The ensemble averages of the times of birth of the first nucleus. *Electrochim. Acta* **2009**, *54*, 879−887.
(38) Ren, H.; Edwards, M. A.; Wang, Y.; White, H. S. Electrochemically Controlled Nucleation of Single CO2 Nanobubbles via Formate Oxidation at Pt Nanoelectrodes. *J. Phys. Chem. Lett.* **2020**, *11*, 1291−1296.

https://doi.org/10.1021/acs.jpcc.2c03973
J. Phys. Chem. C 2022, 126, 20004−20010